On the --fO_2 stability of Fe_4O_5, Fe_5O_6 and Fe_4O_5–rich solid solutions.

Robert Myhill[1,3], Dickson O. Ojwang[1,2], Luca Ziberna[1,3], Daniel J. Frost[1], Tiziana Boffa Ballaran[1], and Nobuyoshi Miyajima[1]

[1]Bayerisches Geoinstitut, Universität Bayreuth, D-95440 Bayreuth, Germany

[2]Inorganic and Structural Chemistry, Department of Materials and Environmental Chemistry, Arrhenius Laboratory, Stockholm University, SE-10691, Stockholm, Sweden

[3]Department of Earth Sciences, University of Bristol, Bristol, BS8 1TH, UK

ABSTRACT

The high pressure phases Fe_4O_5 and Fe_5O_6 have recently been added to the list of known iron oxides. As mixed valence phases, it has been suggested that they could form in the Earth's mantle once the dominant minerals become saturated in ferric iron. The possibility that Fe_4O_5 could exist in the mantle is also supported by the fact that it forms extensive solid solutions with both Mg^{2+} and Cr^{3+}. In this study, we present the results of high pressure and temperature multi-anvil experiments performed between 5 and 24 GPa at 1000–1400 ˚C aimed at constraining the stability field of the Fe_4O_5 phase. We combine these results with published phase equilibria, equation of state and Fe-Mg partitioning data to estimate the thermodynamic properties of Fe_4O_5, Fe_5O_6 and the $(Mg,Fe)_2Fe_2O_5$ solid solution. Using our thermodynamic model the oxygen fugacity at which the high pressure iron oxides become stable are calculated and the redox stability of $(Mg,Fe)_2Fe_2O_5$ in an assemblage of olivine and pyroxene is calculated as a function of the bulk Fe/(Fe+Mg) ratio. Fe_4O_5 and $(Mg,Fe)_2Fe_2O_5$ are stable at oxygen fugacities higher than the diamond stability field and are, therefore, unlikely to be found as inclusions in diamonds. The stability field of Fe_5O_6, on the other hand, extends to oxygen fugacities compatible with diamond formation. Using the Mg–Fe solid solution model, we show that Fe_4O_5-structured phases would be restricted to aluminum-poor environments in the mantle such as dunites or silica-iron oxide-rich sediments transported into the mantle via subduction.

Keywords: Fe_4O_5, Fe_5O_6, thermodynamics, oxygen fugacity, mantle, deep Earth

INTRODUCTION

The oxidation state of the Earth's mantle has an important influence on many transport properties and is strongly related to the speciation of volatile elements with multiple oxidation states such as carbon (Wood et al., 1990; Ballhaus and Frost, 1994; Frost and McCammon, 2008). The oxygen fugacity of the Earth's mantle affects the redox state of volcanic gases, for example, which in turn has influenced the availability of volatile elements at the surface over Earth's history (Delano, 2001). As such, understanding the past and present redox state of the mantle is an important goal. While oxy-thermobarometric methods can be applied to mantle xenoliths to estimate the oxygen fugacity within the top 200 km of the mantle (Wood et al., 1990; Wood 1991; Ballhaus et al., 1991; Stagno et al., 2013), the only samples currently available from greater pressures are mineral inclusions in diamonds. Although a wealth of information is now emerging concerning inclusions within so-called sub-lithospheric diamonds, estimating the redox conditions at which such minerals formed is difficult as redox sensitive equilibria can rarely be identified. The presence of mixed valence iron oxides as inclusions could provide an approximate indication of the oxygen fugacity prevailing in diamond-precipitating fluids in the mantle. For example, almost-pure Fe_3O_4 magnetite inclusions (Stachel et al., 1998; Kaminsky and Wirth 2011) have been found in diamonds and evidence of $(Mg,Fe)Fe_2O_4$ exsolution from ferropericlase (McCammon et al., 1998) has also been observed. Knowledge of the thermodynamic properties of iron oxides at high pressure is an important prerequisite for understanding the fluids in which such oxides form.

Recently a new high-pressure mixed-valence phase with the stoichiometry Fe_4O_5 has been reported as a breakdown product of siderite (Lavina et al., 2011) or magnetite (Woodland et al., 2012) at high pressures. Its crystal structure, determined mainly by powder diffraction and DFT calculations (Lavina et al., 2011; Trots et al., 2012; Guignard and Crichton 2014), has the orthorhombic *Cmcm* space group and consists of layers of edge-sharing FeO_6 octahedra and layers of trigonal prisms alternating along the *c*-axis. With only 50 % of its iron in the trivalent state, this phase should be stable under more reducing conditions than magnetite. It is this property that makes Fe_4O_5 a particularly interesting candidate as a potential host for ferric iron in the Earth's mantle and as a possible gauge for redox processes. Fe_4O_5-structured phases can also accommodate Mg^{2+} and Cr^{3+}, which substitute for Fe^{2+} and Fe^{3+} (Woodland et al., 2013). This solid solution may have been missed in

previous studies; for example, reanalysis of x-ray diffraction analysis of samples from Mg_2SiO_4–Fe_2SiO_4–Fe_3O_4 experiments conducted by Koch et al. (2004) indicate the presence of $(Mg,Fe)_2Fe_2O_5$. The isostructural end-member $Mg_2Fe_2O_5$ was recently synthesized in high-pressure and temperature experiments (Boffa Ballaran et al., 2015). An $Fe_2Cr_2O_5$ end member has also been synthesized (Ishii et al., 2014) although with a different octahedral stacking arrangement compared to Fe_4O_5 and consequently a different space group (Ishii et al., 2014). A wide range of M_4O_5 phase compositions (where M is a cation) may therefore be generated at high pressure and temperature conditions through decomposition reactions involving spinel-structured phases.

A further high-pressure mixed-valence iron oxide with the stoichiometry Fe_5O_6 has been recently reported by Lavina and Meng (2015). Formed between 10 and 20 GPa at ~2000°C, this phase apparently has the same orthorhombic space group as Fe_4O_5 (*Cmcm*). In terms of oxygen fugacity the stability field of Fe_5O_6 should lie between wüstite and Fe_4O_5, and so this new phase may form even if there is insufficient oxygen in the system for Fe_4O_5 to be stable.

Finally, several studies have reported that magnetite transforms to an orthorhombic structure, h-Fe_3O_4, when compressed at room temperature to pressures above 19-27 GPa (Mao et al., 1974; Fei et al., 1999; Huang and Bassett, 1986; Dubrovinsky et al., 2003). The stability field of h-Fe_3O_4 is not well known at high temperature, and sluggish kinetics at low temperatures leads to significant hysteresis (Fei et al., 1999; Lazor et al., 2004).

In this study we investigate the stability of the high pressure Fe_4O_5 and Fe_5O_6 phases. To this end, it is important to consider the following independent reactions:

$$Fe_3O_4 + \text{“FeO”} = Fe_4O_5, \quad [1]$$

$$Fe_4O_5 + \text{“FeO”} = Fe_5O_6, \quad [2]$$

$$2Fe_3O_4 = Fe_4O_5 + Fe_2O_3, \quad [3]$$

$$Fe_3O_4 = \text{h-}Fe_3O_4 \quad [4]$$

Previous work has gone some way towards constraining the positions of these reactions. Schollenbruch et al. (2011), for example, conducted in-situ experiments on magnetite starting compositions, and observed a change in energy-dispersive x-ray diffraction patterns at 10–12 GPa which they attributed to the transformation of magnetite to its high pressure polymorph (Reaction [4]). However, they also observed additional peaks not attributable to h-Fe_3O_4, which suggested the partial breakdown of Fe_3O_4 to some unknown “mystery phase”.

Unfortunately, the quality of their energy-dispersive diffraction patterns did not allow for structural or chemical determination of the phase. Woodland et al. (2012) conducted further *in-situ* synchrotron experiments in the same region of *P-T* space, and discovered that the reaction identified by Schollenbruch et al. (2011) was actually the breakdown of magnetite to Fe_4O_5 and Fe_2O_3 (Reaction [3]).

To examine the stability field of Fe_4O_5 we have performed high pressure and temperature phase equilibria experiments in a multi-anvil apparatus. Using these results together with phase equilibria and compressibility data reported in the literature (Lavina et al., 2011, Schollenbruch et al., 2011, Woodland et al., 2013) we have extracted thermodynamic parameters to describe Fe_4O_5 stability and that of the isostructural Mg-bearing solid-solution $(Mg,Fe)_2Fe_2O_5$. The available data on Fe_5O_6 have also been employed to estimate its thermodynamic properties and stability field. Using the resulting models the conditions at which such phases could form in the mantle are examined.

EXPERIMENTAL AND ANALYTICAL METHODS

High pressure and high temperature experiments to examine the stability field of Fe_4O_5 were conducted in a 500-tonne press using a Walker-type split-cylinder multi-anvil module (Walker et al., 1990) and in 1000 and 1200 tonne presses using Kawai type split-sphere guide blocks. For pressures up to 12 GPa 18-mm edge length Cr_2O_3-doped MgO octahedra were employed as pressure media, which were compressed using tungsten carbide (WC) cubes with 11 mm corner truncations (a so called 18/11-assembly). Higher pressure experiments were performed using 14/8 and 10/4 type assemblies at 16 and 22 GPa respectively. Each pressure medium contained a cylindrical $LaCrO_3$ or graphite furnace, placed inside an outer ZrO_2 sleeve. Further experimental details and pressure calibrations for all assemblies are reported by Keppler and Frost (2005). The temperature was monitored using $W_{97}Re_3$-$W_{75}Re_{25}$ (D-type) thermocouples (with no correction made for the pressure effect on emf) inserted axially inside an alumina tube with the junction in contact with the top of the capsule. This set up ensures that the temperature at the thermocouple junction is essentially identical to that at the top of the sample. We monitored the emf as a function of power during the experiments to check for reaction of the thermocouple. The stability of the emf with

respect to the power drawn by the furnace under peak conditions suggests that there was no significant interaction between the thermocouple and the capsule.

A starting mix of magnetite and iron in a 5:1 molar ratio was used in all experiments, with high pressure Fe_4O_5 formation by the reaction

$$5\ Fe_3O_4 + Fe = 4\ Fe_4O_5. \qquad [5]$$

This mix was chosen to avoid complications involving the non-stoichiometry of wüstite (i.e. $Fe_{1-y}O$ where $y \neq 0$). Magnetite was synthesized from high-purity Fe_2O_3 (99.99 %) powder cold-pressed into pellets and reduced in a 1-atm CO-CO_2 gas-mixing furnace under controlled oxygen fugacity for 16 hours at 1100 ˚C with CO_2/CO ratio of 1.95/0.05, i.e. log fO_2 = - 9.1 (Deines et al., 1974; Chou, 1987). The product was ground in an agate mortar under ethanol with 6-9 µm Fe metal powder, then dried under a heat lamp before loading into cylindrical capsules made from 25 µm thick folded metal foils. The metals used were Re or Mo, which impose different oxygen fugacities when in contact with their respective oxides (ReO_2 and MoO_2). Capsule dimensions depended on the assemblies used: 2 mm Ø × 3.5 mm for the 18/11-type, 1.6 mm Ø × 2.5 mm for the 14/8-type and 1.2 mm Ø × 1.2 mm for the 10/4-type multi-anvil assemblies. Capsules were placed at the center of the assembly within an MgO sleeve and were in contact, on one side, with the junction of the axially inserted thermocouple. Experiments were carried out at pressures between 5 and 22 GPa and temperatures between 1000 and 1400 ˚C. Run durations were between 2 and 20 hours, after which the experiments were quenched by switching off the power to the furnace. Each experiment was subsequently decompressed over several hours (see Table 1 for run details).

The starting material and the recovered run products were characterized by X-ray powder diffraction using a Philips X'Pert Pro X-ray diffraction system operating in reflection mode at 40 kV and 40 mA with $CoK\alpha_1$ (λ = 1.78897 Å) radiation, monochromated with a symmetrically-cut curved Johansson $Ge_{(111)}$ crystal, and equipped with a Philips X'celerator detector. The unit cell edge of the magnetite starting material was a_o = 8.3939(6) Å, in perfect agreement with published values (e.g. Fleet, 1982). The phases identified in the recovered run products are reported in Table 1. Forty to fifty percent of each sample was ground for X-ray diffraction, so the phases reported are representative of the bulk material.

To determine accurately the unit-cell parameter of the Fe_4O_5-phase, selected run products were mixed with Si (NBS standard material #640) as an internal standard. Full pattern profile fitting (Rietveld analysis) was carried out on these samples using the GSAS software package (Larson and von Dreele, 1994) and the Windows interface EXPGUI (Toby, 2001). The resulting unit-cell parameters are reported in Table 2. Powder diffraction patterns of the Fe_4O_5 phase exhibit relatively broad diffraction lines giving rise to uncertainties larger than those indicated by the GSAS program and reported in Table 2.

Three run products, H3551, V739 and S5570, were analysed exclusively by single crystal X-ray diffraction. For this purpose several crystals (more than 30 for each sample) were tested using an Xcalibur diffractometer with MoKα radiation operated at 50 kV and 40 mA, equipped with a CCD detector and a graphite monochromator. All crystals tested could be indexed with the Fe_4O_5 unit cell, although they exhibited very broad peaks in the diffraction spectra (>0.3° in omega profiles).

In order to investigate the origin of the poor crystallinity shown by all Fe_4O_5 single crystals examined, Sample S5648 was polished into a petrographic thin section with a thickness of 30 μm. The thin section was glued onto a 3-mm-sized Mo grid and thinned to electron transparency by Ar-ion bombardment at an 8° angle of incidence and an accelerating voltage of 3.5 keV for 23 hours. The crystals contained in the thin section were characterized by selected area electron diffraction (SAED), TEM imaging, electron diffraction and energy-dispersive X-ray (EDX) on a Philips CM20 FEG (field emission gun) STEM operating at 200 keV. The NORAN Vantage EDX system includes a digital pulse processor, a Ge detector and ultra-thin window, enabling the detection of light elements such as oxygen.

THERMODYNAMIC FRAMEWORK

Thermodynamic modelling of the Fe-O system

Thermodynamic data for Fe, $Fe_{1-y}O$, Fe_3O_4, Fe_4O_5 and Fe_5O_6 are compiled and estimated using experimental data from this study and from the literature. Endmember data for BCC and FCC iron are taken from the 1 bar data of Sundman (1991) and equation of state of Komabayashi (2014). A subregular solid solution model was constructed for wüstite ($Fe_{1-y}O$)

with the endmember compositions $[Fe^{2+}]O$ and $[Fe^{3+}_{2/3}\square_{1/3}]O$. Natural wüstite crystals usually have about 1/3 of the ferric iron cations in tetrahedral-coordination, making an $^{oct}[Fe^{3+}_{1/2}\square_{1/2}]^{tet}[Fe^{3+}]_{1/6}O$ endmember (Hazen and Jeanloz, 1984), but as any constant ratio of octahedral/tetrahedrally-coordinated Fe^{3+} can be chosen to describe this end-member without affecting the configurational entropy on the octahedral site, this complexity is ignored. We also ignore complex changes in defect structure that could affect compressional properties and therefore phase relations (e.g. McCammon and Liu, 1984). In this study, we take the bulk modulus across the solid solution as a constant 152 GPa, which is suitable for more oxidized wustites (y>0.05; McCammon, 1993). The properties of the wüstite solid solution at 1 bar are obtained by fitting the fO_2 across the wüstite solid solution (Bransky and Hed, 1968; Giddings and Gordon, 1972), and the compositions of wüstite in equilibrium with iron as a function of temperature. The resulting model (Table 3) has interaction parameters W(FeO-$Fe_{2/3}O$) = -40121 + 4.27T J/mol and W($Fe_{2/3}O$-FeO) = -4572 + 4.27T J/mol. It produces Gibbs energies of formation similar to those of Stølen and Grønvold (1996), with the added benefit that it can be trivially incorporated into existing solid solution datasets.

Thermodynamic parameters for magnetite and hematite are obtained from dataset 6.2 of Holland and Powell (2011). Although the standard state enthalpy and entropy of these phases is derived from a different model for iron metal, the differences in Gibbs free energy are <1 kJ/mol, which has a negligible effect on the work presented in this paper. The properties of h-Fe_3O_4 are taken from Lazor et al. (2004).

Room temperature equations of state for the high pressure iron oxides are compiled from the results of Lavina et al. (2011) and Woodland et al. (2012) for Fe_4O_5, and Lavina and Meng (2015) for Fe_5O_6 (Table 3). The first derivative of the bulk modulus, K', is fixed at 4 and the second derivative is fixed using the heuristic $-K'_0/K_0$ suggested by Holland and Powell (2011). To extrapolate the volumes to high temperature, we fit the standard state thermal expansivities of Fe_4O_5 and Fe_5O_6 to the single high P-T data points reported by Woodland et al. (2012) and Lavina and Meng (2015). In the absence of heat capacity data, we use the molar sum of values from FeO (stoichiometric wüstite; Holland and Powell, 2011) and magnetite, a technique proposed by Robinson and Haas (1983). Performing the same operation for magnetite using hematite and wüstite reproduces these C_P values to within a couple of percent.

The standard state thermodynamic properties of Fe_4O_5 can be determined either from the phase relations of Reaction [1] reported in this study or from Reaction [3] studied previously (Schollenbruch et al., 2011; Woodland et al., 2012). Here we use Reaction [3] to determine the standard state (1 bar, 298 K) enthalpy of formation and the entropy for Fe_4O_5 and use reaction [1] purely to evaluate the prediction of the resulting model. Reaction [3] was tightly constrained by Schollenbruch et al. (2011), although at the time it was misidentified as the transformation from magnetite to its high-pressure polymorph (Woodland et al., 2012). The enthalpy and entropy thus obtained are given in Table 3.

Reactions related to the formation of Fe_5O_6 are not yet well constrained. It appears that the phase becomes stable above ~10 GPa at both 1200 and 1700 °C (Woodland et al., 2015; Lavina and Meng, 2015), implying that Reaction [2] takes place at a pressure of 9–10 GPa, with a small dP/dT. The standard state enthalpy and entropy are chosen to satisfy these constraints. The small amount of data means that our thermodynamic model for Fe_5O_6 must be considered preliminary. It may require adjustment as more data are published.

Thermodynamic properties of the Fe_4O_5-$Mg_2Fe_2O_5$ solid solution

For the purpose of assessing the stability of the $(Mg,Fe^{2+})_2Fe^{3+}{}_2O_5$ solid solution (Woodland et al., 2013; Boffa Ballaran et al., 2015) we make a first approximation of the thermodynamic properties of the $Mg_2Fe_2O_5$ endmember by examining Fe-Mg partitioning data between $(Mg,Fe^{2+})_2Fe^{3+}{}_2O_5$ and $(Mg,Fe)_2SiO_4$ solid solutions. In this analysis it is assumed that Fe-Mg ordering has little effect on the observed phase relations. The preference of Mg for the trigonal prism site of the $(Mg,Fe^{2+})_2Fe^{3+}{}_2O_5$ stucture (Boffa Ballaran et al., 2015) suggests that this is not a perfect approximation, but is reasonable given the amount of data currently available.

The volume and bulk modulus of $Mg_2Fe_2{}^{3+}O_5$ are taken from currently unpublished data (N. Siersch, pers. comm.). The volume V_0 (5.305 J/bar/mol) is in good agreement with a Vegard's law analysis of the volumes of $(Mg,Fe)_2Fe_2{}^{3+}O_5$ in Woodland et al. (2013). Woodland et al. (2013) also report compositions of coexisting $(Mg,Fe^{2+})_2Fe^{3+}{}_2O_5$ and $(Mg,Fe)_2SiO_4$ olivine, wadsleyite and ringwoodite from experiments performed at 1100°C between 9 and 16 GPa. These data have been used to constrain the properties of the solid solution. The exchange of

Fe^{2+} and Mg between these phases can be described on a single site mixing basis by the equilibrium,

$$MgFeO_{2.5} + FeSi_{0.5}O_2 = Fe_2O_{2.5} + MgSi_{0.5}O_2 \quad [6]$$

The standard state Gibbs free energy for this equilibrium when the $(Mg,Fe)_2SiO_4$ phase is olivine is described by,

$$\Delta G^{\circ}_{(P,T)} = -RTln\left(\frac{a^{oxide}_{Fe_2O_{2.5}} a^{olivine}_{MgSi_{0.5}O_2}}{a^{oxide}_{MgFeO_{2.5}} a^{olivine}_{FeSi_{0.5}O_2}}\right) \quad [7]$$

If we assume, based on the small difference in ionic radius between Mg and Fe^{2+}, that mixing is ideal in $(Mg,Fe)_2Fe_2^{3+}O_5$, then,

$$RTln\left(\frac{a^{oxide}_{Fe_2O_{2.5}} a^{olivine}_{MgSi_{0.5}O_2}}{a^{oxide}_{MgFeO_{2.5}} a^{olivine}_{FeSi_{0.5}O_2}}\right) = RTln\left(\frac{X^{ox}_{Fe} X^{ol}_{Mg}}{X^{ox}_{Mg} X^{ol}_{Fe}}\right) + W^{ol}_{Fe-Mg}\left(2X^{ol}_{Fe} - 1\right) \quad [8]$$

where, for example $X^{ox}_{Fe} = Fe^{2+\cdot}/(Mg + Fe^{2+\cdot})$ and W^{ol}_{Fe-Mg} is a Margules interaction parameter. In this study, we find the best fitting standard state enthalpy of $Mg_2Fe_2O_5$ from the observed compositions of coexisting olivine and $(Mg,Fe)_2Fe_2O_5$, then use this value to model the compositions of wadsleyite and ringwoodite coexisting with $(Mg,Fe)_2Fe_2O_5$.

RESULTS

Microstructures in Fe_4O_5

Since all powder diffraction patterns and single-crystal diffraction profiles collected for Fe_4O_5 exhibited broad diffraction lines, Sample S5648 (12 GPa, 1300 ˚C) was analyzed by TEM in order to obtain some insight into the nature of defects present in this phase. Bright field TEM images of the Ar-ion milled sample show fringes of Fe_4O_5 with fine parallel exsolution lamellae of Fe_3O_4 (Fig. 1a). Indexing of the electron diffraction patterns revealed lamellar twinning of the magnetite phase. Magnetite crystals with numerous polysynthetic twins parallel to {311} are also observed in Sample S5640 (22 GPa, 1000 ˚C). The relationship between the two oxides is topotactic; the lattice planes {311} for Fe_3O_4 and (002) for Fe_4O_5 are coplanar and the reciprocal spots in the selected area electron diffraction

pattern are perpendicular to the plane of the lamellae (Fig. 1b). The presence of this lamellar intergrowth is likely to be the cause of the x-ray diffraction line broadening seen for Fe_4O_5 profiles.

Experimental phase relations of Fe_4O_5

The experimentally determined phase relations for Fe_4O_5 (+ δO) are shown in Figure 2. Below ~8 GPa the stable assemblage is a mixture of wüstite and magnetite. The Fe_4O_5 formation reaction [1] was pressure-bracketed between 7 and 8 GPa at both 1000°C and 1100°C and temperature-bracketed between 1200 °C and 1300 °C at 8 GPa. The dP/dT slope of the transformation is therefore small, but probably slightly positive. The coexistence of Fe_4O_5 and a small amount of magnetite at >8 GPa implies slight oxidation of the starting material, either prior to or during the experiment. The presence of twinned magnetite in run (S5640) from 22 GPa, discussed above, is most consistent with back-transformation with accompanying oxidation of Fe_4O_5 during either decompression or grinding for powder x ray diffraction analysis. As will be shown later, with respect to fO_2, the stability fields of both magnetite and Fe_4O_5 are several log units higher than the Mo-MoO_2 oxygen buffer. This is consistent with the formation of small amounts of MoO_2 in both experiments where molybdenum capsules were employed. Similarly, the fO_2 of the Re-ReO_2 buffer passes through the stability field of Fe_4O_5, which is consistent with the appearance of ReO_2 in experiments that used rhenium capsules.

At 1250 ˚C (6 GPa) and 1300 ˚C (8 GPa) a narrow corona of melt formed at the wall of the capsule around the wüstite plus magnetite assemblage (see Supplementary Figure 1). The melting points of both phases should be well over 1600 °C at this pressure (Lindsley, 1966) and there is no eutectic between these phases, at least at 1 bar. The presence of Re metal within the quenched melt suggests that melting was fluxed by ReO_2. Alternatively, hydrogen diffusion from the assembly driven by oxygen chemical potential gradients (e.g. Eugster, 1957) could have caused the observed melting.

Phase relations in the Fe-O system

A *P-fO*$_2$ diagram for the Fe-O system calculated at 1200 °C is shown in Figure 3. The stabilities of the iron-oxides are compared with curves calculated for the Re-ReO$_2$, Mo-MoO$_2$, EMOD (enstatite + magnesite = olivine + diamond), FMQ (fayalite = magnetite + quartz) and QIF (quartz + Fe = fayalite) oxygen buffers (Holland and Powell 2011; Holland et al., 2013). The metal-metal oxide buffer data are taken from Barin (1989) at 1 bar, with estimates for the PVT equations of state taken from the literature (see Supplementary Materials).

In appropriate bulk compositions, Fe_4O_5 and Fe_5O_6 are predicted to coexist over broad ranges of pressure and temperature, with the equilibrium between these iron-oxides lying 1-2 log units below the metastable extension of the FMQ buffer. The Fe_4O_5 stability field is consistently above the EMOD buffer, implying that it is unlikely to be found as an inclusion within a mantle diamond. Fe_5O_6, on the other hand, is predicted to be stable within the forsterite + diamond stability field. The range of oxygen fugacities over which these mixed valence iron oxides are stable expands with increasing pressure from ~3 log units at 12 GPa to ~6 log units at 21 GPa. The Fe_5O_6 field expands mostly at the expense of the wüstite field. Although there are uncertainties in the model resulting from the fact that the formation pressure of Fe_5O_6 is not well constrained as a function of temperature, this has little influence on the prediction that the wüstite field should narrow with pressure because this is a function of the volumes of the phases involved which are well constrained. Although the wüstite field narrows, the model predicts that at pressures higher than 24 GPa the wüstite-Fe_5O_6 and the wüstite-Fe boundary become essentially parallel in *P-fO*$_2$ space, ensuring that the wüstite stability field persists to high pressures, in accordance with experimental data (e.g. Ozawa et al., 2011).

Equilibrium between (Fe,Mg)$_2$Fe$_2$O$_5$ and the olivine polymorphs

Figure 4 shows the exchange coefficient K_D for equilibrium [6], where

$$K_D = \left(\frac{X_{Fe}^{ox} X_{Mg}^{ol}}{X_{Mg}^{ox} X_{Fe}^{ol}}\right) \qquad [9]$$

plotted from the data of Woodland et al. (2013) as a function of the $(Mg,Fe)_2Fe_2^{3+}O_5$ $Mg/(Mg+Fe^{2+})$ ratio for exchange with olivine, wadsleyite and ringwoodite. From fitting equation [7] to the data for olivine using values of W_{Fe-Mg}^{ol} from Holland et al., (2013) an

estimate can be made for the standard state Gibbs free energy of equilibrium [6] at the *P-T* conditions of the experiments. Using thermodynamic data for Fe_4O_5 determined in this study and data on olivine from Holland et al., (2013), it is then possible to make an estimate of the Gibbs free energy of formation of $Mg_2Fe_2^{3+}O_5$ at 1100°C and 10 GPa. Finally, the formation of pure $Mg_2Fe_2^{3+}O_5$ at 1550°C, 15 GPa (Boffa Ballaran et al., 2015) constrains the standard state entropy to be at least 54 J/K/mol from the reaction per+hem → $Mg_2Fe_2^{3+}O_5$.

As shown in Figure 4, the resulting model provides an excellent fit to the olivine data, but there are discrepancies in calculated wadsleyite and ringwoodite compositions. We note that the equilibrium K_D values reported by Woodland et al. (2013) are rather scattered and do not exhibit the expected variation with pressure and Mg content. This may reflect disequilibrium or equilibration at different oxygen fugacities, which is known to influence Fe-Mg partitioning behaviour in wadsleyite and ringwoodite (Frost and McCammon, 2009). Although Woodland et al. (2013) report very low ferric iron concentrations in their wadsleyites and ringwoodites, these are based on microprobe totals, and therefore subject to quite large uncertainties which are heavily dependent on the analysed mineral phases and standards used for calibration.

DISCUSSION

The breakdown of metastable Fe_4O_5

At room pressure, Fe_4O_5 is a highly metastable phase prone to decomposition at relatively low temperatures (Trots et al., 2012). In this study, we show that Fe_4O_5 breaks down under oxidising conditions by forming lamellar intergrowths of {311}-twinned Fe_3O_4. We note that wüstite is not associated with the formation of this twinned magnetite, requiring bulk oxidation of the sample. The most likely explanation for our observations is that magnetite formed while the sample was in contact with oxygen in the atmosphere or fluids used during preparation (epoxy, ethanol, water).

We also suggest that the unusual {311} twin in magnetite can be used to identify crystals which were once Fe_4O_5. We note that this form of twinning has been recognised in magnetite coexisting with ringwoodite in samples recovered from quenched experiments performed at

21 GPa and 1600 ˚C by Frost et al. (2001), and in samples recovered from the high pressure Fe_3O_4 experiments conducted by Schollenbruch et al. (2011).

The stability of Fe_4O_5 and implications for h-Fe_3O_4

The thermodynamic data for Fe_4O_5 derived using experimental data on the magnetite-out reaction (Reaction [3]) provide an excellent fit to the observed *P-T* position of the Fe_4O_5-in reaction (Reaction [1]; Figure 2). The position of the magnetite-out reaction is very similar to the extrapolated Fe_3O_4 → h-Fe_3O_4 reaction proposed by Lazor et al. (2004). It is therefore important to discuss the stability of the high pressure polymorph of magnetite.

Experimental investigations suggest that Fe_4O_5 + Fe_2O_3 is more stable than h-Fe_3O_4 up to at least ~16 GPa at 1300 °C (Woodland et al., 2012). h-Fe_3O_4 has typically been investigated at much lower temperatures; for example, it was found to be stable relative to magnetite down to 24 GPa at 550 °C (Fei et al., 1999). Under these conditions, it is quite possible that the formation of Fe_4O_5 + Fe_2O_3 may be kinetically hindered. The equation of state of h-Fe_3O_4 according to Lazor et al. (2004) indicates that the volume of h-Fe_3O_4 is consistently higher than that of 0.5(Fe_4O_5 + Fe_2O_3) above ca. 200 °C, which would preclude h-Fe_3O_4 as a stable high pressure, high temperature phase. However, the equation of state of Lazor et al. lacks a Landau-type transition in high-magnetite, which does exist in magnetite. This transition stabilises magnetite at high temperature relative to h-Fe_3O_4, explaining the discrepancy between the location of the Fe_3O_4 → h-Fe_3O_4 reaction in this study (Figure 2; 16 GPa at 900 °C) and in Lazor et al. (12 GPa at 900 °C). If high-magnetite undergoes a Landau-type transition similar to that of its low-pressure polymorph, it does become stable at high temperature, but suggests that h-Fe_3O_4 is metastable relative to Fe_4O_5 and Fe_2O_3 at low temperature. Clearly the high-temperature thermal properties of high-magnetite (and Fe_4O_5) are worthy of further study to better constrain the stability of h-Fe_3O_4.

The stability of $(Mg,Fe)_2Fe_2O_5$ relative to upper mantle phases

The compositions of upper mantle rocks generally place them within ±2 log units of the FMQ oxygen buffer at low pressures (Frost and McCammon, 2008). However, minerals such as clinopyroxene and garnet incorporate increasing quantities of ferric iron into their structures at higher pressures, which has the effect of decreasing the oxygen fugacity relative to the

FMQ buffer (Rohrbach et al., 2007; 2011). Rocks from the deepest portions of the cratonic lithosphere record values that are over 3 log units below FMQ (Stagno et al., 2013), and this trend is expected to result in the saturation of metallic iron in the deep upper mantle (Rohrbach et al., 2011).

The upper mantle is comprised primarily of peridotitic rocks, which are not well-described by the Fe-O system (Figure 3). We extend our analysis to peridotitic assemblages by investigating the following redox reaction between the iron silicate endmembers of common mantle phases,

$$8\ Fe_2SiO_4\ (ol,wad,rw) + O_2 \rightarrow 8\ FeSiO_3\ (opx,cpx,gt,aki,pv) + 2\ Fe_4O_5 \quad [10]$$

accounting for the fact that these minerals are solid solutions.

We first investigate the MgO-FeO-Fe_2O_3-SiO_2 (FMSO) system, which is the most mantle-like system under which Fe_4O_5-structured phases have been experimentally produced (Koch et al., 2004, Woodland et al., 2013). Figure 5 illustrates the effect of pressure on oxygen fugacity for an olivine-orthopyroxenite containing $(Mg,Fe)_2Fe_2O_5$ at 1400 °C. This diagram reveals that at high magnesium contents, $(Mg,Fe)_2Fe_2O_5$ is unstable relative to hematite. For example, a solid solution with 20–30 mol% $Mg_2Fe_2O_5$ in a peridotite with $Mg/(Mg+Fe) \sim 0.9$ imposes redox conditions that are more oxidising than the (metastable) QFM buffer. The stabilisation of $(Mg,Fe)_2Fe_2O_5$ in such a simple system would, therefore, require rocks which have remained isolated from mantle-derived fluids (which would impart lower oxygen fugacities on the system). However, the limited ability of olivine and HP-clinopyroxene to accommodate ferric iron means that these unusually high oxygen fugacities would not require unusually high ferric iron contents; primitive mantle typically has $Fe^{3+}/\sum Fe \sim 0.03$ (Canil et al., 1994).

The FMSO system accounts for the majority of mafic and ultramafic bulk compositions, but other components are also important for predicting high-pressure phase relations. Probably the most important in this study is alumina, which stabilises garnet, the dominant host of ferric iron in the deep upper mantle (Rohrbach et al., 2007; Rohrbach et al., 2011). Even extremely depleted dunites contain non-negligible quantities of alumina in pyroxene and

other minor phases (Godard et al., 2008). Unless $(Mg,Fe)_2Fe_2O_5$ solid solutions can also accept significant quantities of alumina, they will be destabilised by the following reaction:

$$Fe_4O_5 + 5FeSiO_3 \text{ (opx, gt, aki, pv)} \rightarrow Fe_3Fe_2Si_3O_{12} \text{ (gt)} + 2Fe_2SiO_4 \text{ (ol,wad,rw)} \quad [11]$$

Insights into the capacity of garnets to destabilise mixed-valence oxides can be gained from calculating the ferric-iron contents of garnets at the oxygen fugacities where $(Mg,Fe)_2Fe_2O_5$ is stable. In Figure 6, we calculate the ferric iron and pyrope content of FMASO garnets (White et al., 2014; updated version in the THERMOCALC database) corresponding to the 0.9 Mg/(Mg+Fe) contour plotted in Figure 5. The calculated ferric contents are extremely high; the formation of such khoharite-rich ($Mg_3Fe_2Si_3O_{12}$) garnets (and, by extension, $(Mg,Fe)_2Fe_2O_5$) in normal alumina-bearing peridotite would require exceptionally oxygen-rich source rocks. The implication is that in the deep Earth, $(Mg,Fe)_2Fe_2O_5$ must be restricted to rocks with aluminium-poor bulk compositions.

We are currently unable to assess the potential stability of Fe_5O_6-structured phases in the mantle, as the stability of this phase will also depend on the extent and nature of the Mg-bearing solid solution, and on the potential amount of alumina incorporation. If neither Fe_4O_5 nor Fe_5O_6 can substitute ferric iron for aluminium, their presence will be restricted to aluminium-poor lithologies, regardless of oxidation state.

Conclusions

In this study, we have accurately constrained the stability of the new high pressure phase Fe_4O_5 under *P-T* conditions relevant to the upper mantle through multi-anvil experiments and subsequent analysis of run products. Microtextural analysis shows the quenched phase to be highly metastable, and to display a lamellae intergrowth of magnetite that is likely formed during decompression or sample preparation. This probably explains the broad x-ray diffraction lines observed for this phase. Using the phase equilibria results, and those from previously published studies, we have constructed thermodynamic models to describe the stability of Fe_4O_5 and Fe_5O_6, and Mg-bearing Fe_4O_5. We use these models to calculate the oxygen fugacities at which these phases will be in equilibrium with other iron oxides, and with mantle minerals.

The results show that the stabilisation of $(Mg,Fe)_2Fe_2O_5$ within an assemblage containing olivine, olivine polymorphs and pyroxene requires oxygen fugacities >FMQ, which exceed those in the lithosphere, as estimated from mantle xenoliths (Stagno et al., 2013), and very likely those in the convecting mantle based on the iron redox state of mid ocean ridge basalts (Cottrell and Kelley, 2013). Furthermore, even if this oxygen fugacity were obtained, $(Mg,Fe)_2Fe_2O_5$ could only form if the bulk composition is extremely Al_2O_3-depleted, otherwise unrealistically large bulk $Fe^{3+}/\sum Fe$ ratios would be required. This would limit $(Mg,Fe)_2Fe_2O_5$ stability to lithologies such as highly-oxidized dunites and sediments. It has been proposed that banded iron formations could have been subducted into the mantle in the Archean (Dobson et al., 2005). Fe_4O_5 would have very likely formed within such aluminium-poor lithologies as they reached pressures >8 GPa, providing they did not interact with reducing fluids or melts.

Our modelling of the newly discovered phase Fe_5O_6 suggests that it may be stable at mantle oxygen fugacities. However, we stress that there is currently very little experimental data on the endmember, and no data on solid solutions. In terms of determining whether this phase can exist in the mantle, a key issue will be to constrain the extent to which this phase forms solid solutions with Mg and Cr.

Acknowledgements

This study was supported by a Humboldt Fellowship awarded to RM and the ERC Advanced Grant ACCRETE project (Contract Number 290568).

The authors would like to thank Stefan Ubelhack and Heinz Fischer for assembly and capsule cutting and Hubert Schulze and Raphael Njul for the preparation of run products. They also thank Chris Ballhaus and two anonymous reviewers for their insightful comments which helped to significantly improve the manuscript.

References

Ballhaus, C., Frost, B.R. (1994). The generation of oxidised CO_2-bearing basaltic melts from reduced CH_4-bearing upper mantle sources. Geochim. Cosmochim. Acta 58: 4431-4440

Ballhaus, C., Berry, R.F., Green, D.H. (1991). High pressure experimental calibration of the olivine-orthopyroxene-spinel oxygen geobarometer: implications for the oxidation state of the upper mantle. Contrib. Mineral. Petrol. 107:27-40

Barin, I. (1989), Thermochemical Data of Pure Substances, Volume VII. VCH Weinheim FRG.

Boffa Ballaran T., Uenver-Thiele L., Woodland A.B. (2015) Complete substitution of Fe^{2+} by Mg in Fe_4O_5: The crystal structure of the $Mg_2Fe_2O_5$ end-member. Am. Mineral., 100, 628-632.

Bransky, I., and Hed, A. Z. (1968). Thermogravimetric Determination of the Composition-Oxygen Partial Pressure Diagram of Wustite ($Fe_{1-y}O$). Journal of the American Ceramic Society, 51, 231-231.

Canil, D., and O'Neill, H. S. C. (1996). Distribution of ferric iron in some upper-mantle assemblages. Journal of Petrology, 37, 609-635.

Canil, D., O'Neill, H. S. C., Pearson, D. G., Rudnick, R.L., McDonough, W.F., Carswell, D.A. (1994). Ferric iron in peridotites and mantle oxidation states, 123, 205-220.

Chou, I. M. (1987) Oxygen buffer and hydrogen sensor techniques at elevated pressures and temperatures. In: Ulmer GC, Barnes HC Jr (eds) Hydrothermal experimental techniques. Wiley, New York. 60-99.

Cottrell, E. and Kelley, K.A. (2013) Redox Heterogeneity in Mid-Ocean Ridge Basalts as a Function of Mantle Source. Science, 340, 1314-1317.

Deines, P., R. H. Nafziger, G. C. Ulmer., and Woermann, E. (1974) T-fO_2 tables for selected gas mixtures in the C-H-O system at one atmosphere total pressure. College Earth and Mineral Sci. Bull. Exp. Station, 88, 1-129

Delano, J.W. (2001) Redox history of the Earth's interior since 3900 Ma: implications for prebiotic molecules. Orig. Life Evol. Bios 31, 311-341

Dubrovinsky, L. S., Dubrovinskaia, N. A., McCammon, C., Rozenberg, G. Kh., Ahuja, R., Osorio-Guillen, J. M., Dmitriev, V., and Weber, H-P., Le Bihan, T. and Johansson, B. (2003) The structure of the metallic high-pressure Fe_3O_4 polymorph:experimental and theoretical study. Journal of Physics: Condensed Matter, 15, 7697-7706.

Eugster, H. P. (1957). Heterogeneous reactions involving oxidation and reduction at high pressures and temperatures. The Journal of Chemical Physics, 26, 1760-1761.

Evrard, O., Malaman, B., Jeannot, F., Courtois, A., Alebouyeh, H., and Gerardin, R. (1980) Mise en évidence de $CaFe_4O_6$ et détermination des structures cristallines des ferrites de calcium $CaFe_{2+n}O_{4+n}$ (n = 1, 2, 3): nouvel exemple d'intercroissance. Journal of Solid State Chemistry, 35, 112-119.

Fei, Y., Frost, D. J., Mao, H. K., and Prewitt, C. T. Haüsermann D (1999) In situ structure determination of the high-pressure phase of Fe3O4. American Mineralogist, 84, 203-206.

Fleet, M. E. (1982) The structure of magnetite: Two annealed natural magnetites, $Fe_{3.005}O_4$ and $Fe_{2.96}Mg_{0.04}O_4$. Acta Crystallography, C40, 1491-1493

Frost, D. J., Langenhorst, F. and Van Aken, P. A. (2001) Fe-Mg partitioning between ringwoodite and magnesiowüstite and the effect of pressure, temperature and oxygen fugacity. Phys Chem minerals 28, 455-470

Frost, D. J. (2003) Fe^{2+}-Mg partitioning between garnet, magnesiowüstite, and $(Mg, Fe)_2SiO_4$ phases of the transition zone. American Mineralogist, 88, 387-397.

Frost, D. J., Liebske, C., Langenhorst F., McCammon C. A., Tronnes, R. G. and Rubie D. C. (2004) Experimental evidence for the existence of iron-rich metal in the Earth's lower mantle. Nature 428, 409-412

Frost, D. J., and McCammon, C. A. (2008). The redox state of Earth's mantle. Ann. Rev. Earth Planet. Sci., 36, 389-420.

Frost, D. J. and McCammon, C. A. (2009) The effect of oxygen fugacity on the olivine to wadsleyite transformation: Implications for remote sensing of mantle redox state at the 410 km seismic discontinuity. Am. Min. 94, 872-882

Giddings, R. A., and Gordon, R. S. (1973). Review of Oxygen Activities and Phase Boundaries in Wustite as Determined by Electromotive- Force and Gravimetric Methods. Journal of the American Ceramic Society, 56(3), 111-116.

Hazen, R. M. and Jeanloz, R. (1984). Wüstite ($Fe_{1-x}O$): A review of its defect structure and physical properties. Reviews of Geophysics, 22, 37-46.

Heinemann, S., Sharp, T. G., Seifert, F. and Rubie, D. C. (1997). The cubic-tetragonal phase transition in the system majorite ($Mg_4Si_4O_{12}$)–pyrope ($Mg_3Al_2Si_3O_{12}$), and garnet symmetry in the Earth's transition zone. Physics and Chemistry of Minerals, 24, 206-221.

Holland, T. J. B., Powell, R. (2011) An improved and extended internally consistent thermodynamic dataset for phases of petrological interest, involving a new equation of state for solids. Journal of Metamorphic Geology 29, 333-383.

Holland, T. J., Hudson, N. F., Powell, R., and Harte, B. (2013). New thermodynamic models and calculated phase equilibria in NCFMAS for basic and ultrabasic compositions through the transition zone into the uppermost lower mantle. Journal of Petrology, 54, 1901-1920.

Huang, E., and Bassett, W. A. (1986). Rapid determination of Fe3O4 phase diagram by synchrotron radiation. Journal of Geophysical Research: Solid Earth (1978–2012), 91(B5), 4697-4703.

Ishii, T., Kojitani, H., Tsukamoto, S., Fujino, K., Mori, D., Inaguma, Y., Tsujino, N., Yoshino, T., Yamazaki, D., Higo, Y., Funakoshi, K., and Akaogi, M. (2014) High-pressure phase transitions in $FeCr_2O_4$ and structure analysis of new post-spinel $FeCr_2O_4$ and $Fe_2Cr_2O_5$ phases with meteoritical and petrological implications. American Mineralogist, in press.

Kaminsky, F.V., Wirth, R. (2011) Iron carbide inclusions in lower-mantle diamond from Juina Barzil. Canadian Mineralogist, 49, 555-572

Keppler, H., and Frost, D. J. (2005) Introduction to minerals under extreme conditions. In: Miletich R (ed) Mineral behaviour at extreme conditions EMU notes in mineralogy 7. Eötvös University Press, Budapest, pp 1-30

Koch, M., Woodland, A. B., and Angel, R. J. (2004) Stability of spinelloid phases in the system Mg_2SiO_4-Fe_2SiO_4-Fe_3O_4 at 1100˚C and up to 10.5 GPa. Physics of the Earth and Planetary Interiors, 143, 171-183

Komabayashi, T. (2014). Thermodynamics of melting relations in the system Fe- FeO at high pressure: Implications for oxygen in the Earth's core. Journal of Geophysical Research: Solid Earth, 119(5), 4164-4177.

Larson, A.C and von Dreele, R.B. (1988) GSAS manual. Los Alamos National Laboratory, report LAUR, 86-748

Lavina, B., Dera, P., Kim, E., Meng, Y., Downs, R. T., Weck P. F., Sutton, S. R., and Zhao, Y. (2011) Discovery of the recoverable high-pressure iron oxide Fe4O5. Proceedings of the National Academy of sciences (PNAS), 108, 17281-17285

Lavina, B., and Meng, Y. (2015) Unraveling the complexity of iron oxides at high pressure and temperature: Synthesis of Fe5O6. Science Advances 1.5, e1400260.

Lazor, P., Shebanova, O. N., and Annersten, H. (2004) High-pressure study of stability of magnetite by thermodynamic analysis and synchrotron X-ray diffraction. Journal of Geophysical Research: Solid Earth 109, B5.

Lindsley, D. H. (1966) Pressure-temperature relations in the system FeO-SiO_2. Year Book Carnegie Inst. Washington, 65, 226– 230.

McCammon, C. (1993). Effect of pressure on the composition of the lower mantle end member Fe_xO. Science, 259, 66-68.

McCammon CA, Chinn IL, Gurney JJ, McCallum M (1998) Ferric iron content of mineral inclusions in diamonds from George Creek, Colorado determined using Mössbauer spectroscopy. Contrib Miner Petrol 133, 30–37

McCammon, C. A., and Liu, L. G. (1984). The effects of pressure and temperature on nonstoichiometric wüstite, Fe_xO: The iron-rich phase boundary. Physics and Chemistry of Minerals, 10, 106-113.

Mao, H. K., Takahashi, T., Bassett, W. A., Kinsland, G. L., and Merrill, L. (1974). Isothermal compression of magnetite to 320 KB. Journal of Geophysical Research, 79(8), 1165-1170.

Ozawa, H., Takahashi, F., Hirose, K., Ohishi, Y., and Hirao, N. (2011). Phase transition of FeO and stratification in Earth's outer core. Science, 334(6057), 792-794.

Robinson, G. R., and Haas, J. L. (1983) Heat capacity, relative enthalpy, and calorimetric entropy of silicate minerals; an empirical method of prediction. American Mineralogist, 68, 541-553.

Rohrbach, A., Ballhaus, C., Golla-Schindler, U., Ulmer, P., Kamenetsky, V.S, Kuzmin, D.V. (2007) Metal saturation in the upper mantle. Nature, 449, 456-458.

Rohrbach, A., Ballhaus, C., Ulmer, P., Golla-Schindler, U., Schönbohm, D. (2011) Experimental Evidence for a Reduced Metal-saturated Upper Mantle. Journal of Petrology, 52, 717-731.

Schollenbruch, K., Woodland, A. B., Frost D. J., Wang, Y., Sanehira, T., and Langenhorst, F. (2011) In situ determination of the spinel-post -spinel transition in Fe_3O_4 at high temperature and pressure by synchrotron X-ray diffraction. American Mineralogist, 96, 820-827.

Stachel T, Harris JW, Brey GP (1998) Rare and unusual mineral inclusions in diamonds from Mwadui, Tanzania. Contrib Miner Petrol 132, 34–47.

Stagno, V., Ojwang, D. O., McCammon, C. A., and Frost, D. J. (2013). The oxidation state of the mantle and the extraction of carbon from Earth's interior. Nature, 493, 84-88.

Stølen, S., and Grønvold, F. (1996). Calculation of the phase boundaries of wüstite at high pressure. Journal of Geophysical Research: Solid Earth,101, 11531-11540.

Sundman, B. (1991). An assessment of the Fe-O system. Journal of Phase Equilibria, 12(2), 127-140.

Toby, B. H. (2001) EXPGUI, a graphical user interface for GSAS. Journal of Applied Crystallography, 34, 210-213

Trots, D. M., Kurnosov, A., Woodland, A. B., and Frost, D. J. (2012) The thermal breakdown of Fe_4O_5 at ambient pressure. European Mineralogical conference, Vol. 1, EMC2012-556-1

Walker, D., Carpenter, M. A., Hitch, C. M. (1990) Some simplifications to multianvil devices for high-pressure experiments. American Mineralogist, 75, 1020-1028

White, RW, Powell, R and Clarke, GL (2002) The interpretation of reaction textures in Fe-rich metapelitic granulites of the Musgrave Block, central Australia: constraints from mineral equilibria calculations in the system K_2O-FeO-MgO-Al_2O_3-SiO_2-H_2O-TiO_2-Fe_2O_3. Journal of Metamorphic Geology, 20, 41-55.

White, R. W., Powell, R., Holland, T. J. B., Johnson, T. E. and Green, E. C. R. (2014). New mineral activity–composition relations for thermodynamic calculations in metapelitic systems. Journal of Metamorphic Geology, 32, 261-286.

Woodland, A. B., and O'Neill, H. S. C. (1993). Synthesis and stability of $Fe^{2+}_3Fe^{3+}_2Si_3O_{12}$ garnet and phase relations with $Fe_3Al_2Si_3O_{12}$–$Fe^{2+}_3Fe^{3+}_2Si_3O_{12}$ solutions. American Mineralogist, 78, 1002-1015.

Woodland, A. B., Frost, D. J., Trots, D. M., Klimm, K., Mezouar, M. (2012) In situ observation of the breakdown of magnetite (Fe_3O_4) to Fe_4O_5 and hematite at high pressures and temperatures. American Mineralogist, 97, 1808–1811

Woodland, A. B., Schollenbruch, K., Koch, M., Boffa Ballaran, T., Angel, R. J., Frost, D. J. (2013) Fe_4O_5 and its solid solutions in several simple systems. Contrib Miner Petrol 166, 1677-1686

Woodland, A. B., Uenver-Thiele, L., Boffa Ballaran, T. (2015) Synthesis of Fe_5O_6 and the high-pressure stability of Fe^{2+}-Fe^{3+}-oxides related to Fe_4O_5. Goldschmidt Abstracts.

Wood, B.J., Bryndzia, L.T., Johnson, K.E. (1990). Mantle oxidation state and its relationship to tectonic environment and fluid speciation. Science 248: 337-45

Wood, B.J. (1991). Oxygen barometry of spinel peridotites. In Oxide Minerals: Petrologic and Magnetic significance, ed. DH Lindsley. Rev. Mineral., 25:417-31. Washington, DC: Mineral. Soc. Am. 508 pp

Figure captions

Figure 1 (a). Bright field TEM image and corresponding electron diffraction pattern (inset) of Fe_3O_4 and Fe_4O_5 from run S5648. The images reveal the presence of nanometer-scale lamellae. **(b)** The same electron diffraction pattern as in (a), reproduced at a larger scale to clearly show the topotactic relationship between Fe_3O_4 and Fe_4O_5 phases. The electron diffraction pattern is taken across the lamellar-twin intergrowth imaged with the incident electron beam along <110> and <-12-1> zone axes of Fe_4O_5 and Fe_3O_4 respectively.

Figure 2. Isochemical *P-T* phase diagram for the bulk composition Fe_4O_5+Re+δO. The mineral assemblages observed in the run products of the high pressure experiments (this study) are reported as wedges in the circular symbols. Triangular symbols indicate the reaction observed *in-situ* by Schollenbruch et al. (2011) and identified as the magnetite-out reaction by Woodland et al. (2012). The solid lines correspond to univariant reactions

calculated using the thermodynamic data described in the main text. The dashed black line corresponds to the part of the calculated $Fe_3O_4 \rightarrow Fe_4O_5 + Fe_2O_3$ that is metastable at the Re-ReO_2 buffer. The dashed grey line is the $Fe_3O_4 \rightarrow$ high-Fe_3O_4 reaction (Lazor et al., 2004). We find high-Fe_3O_4 to be unstable relative to a mixture of $Fe_4O_5 + Fe_2O_3$. MOx stands for the metal oxides of Re and Mo.

Figure 3. Stable phases in the Fe-O system as a function of pressure and oxygen fugacity at 1200 ˚C. The black dotted lines correspond to the Re-ReO_2, and Mo-MoO_2 buffers. The grey dashed lines are the (mostly) metastable QFM and QFI buffers. The solid grey lines delineate different regions of the stable QFM / QFI – like buffers. The Fe_2SiO_4 polymorphs are only stable within their labelled fields. Outside these fields, they will break down into iron/iron oxide and one of the SiO_2 polymorphs.

Figure 4. Mg content in $(Mg,Fe)_2Fe_2O_5$ versus the Fe/Mg Kd with coexisting olivine polymorphs, taken from the data of Woodland et al. (2013). Experimental pressures in GPa are provided next to each data point. All data were collected at 1100°C. Curves show the fit of equation [7] using the parameters described in the text.

Figure 5. Modelled pressure-fO_2 relations for $(Mg,Fe)_2SiO_4$–$(Mg,Fe)_2Si_2O_6$–$(Mg,Fe)_2Fe_2O_5$ at 1400 ˚C. Compositional contours are molar Mg/(Mg+Fe) fractions in the ol+HP-cpx assemblage (i.e. the bulk Mg# when quantities of $(Mg,Fe)_2Fe_2O_5$ are negligible). $(Mg,Fe)_2Fe_2O_5$ in the lower part of the diagram is metastable with respect to $(Mg,Fe^{2+},Fe^{3+})O$ and potentially $(Mg,Fe)_3Fe_2O_6$. Mg and Si solubility in hematite is ignored, as is the possibility of ferric-iron-bearing spinels, which would exist between the hematite (hem) and $(Mg,Fe)_2Fe_2O_5$–bearing fields. At the highest pressures, HP-clinopyroxene is metastable with respect to majoritic garnet. The 'EMOD' (HP-clinoenstatite-magnesite-olivine/wadsleyite/ringwoodite-diamond) and metastable QFM (quartz-fayalite-magnetite) buffers are also shown.

Figure 6. FMASO (py-alm-kho) garnet compositions corresponding to the 0.9 Mg/(Mg+Fe) contour in Figure 5. Such ferric-rich compositions imply an extremely oxidised source (see discussion in text).

Table 1. Syntheses conditions and phases present in the run products identified by X-ray diffraction. V, H and S refer to experimental run numbers correspond to the 500, 1000 and 1200t multi-anvil presses, respectively. # Mo capsule. *$LaCrO_3$ heaters. TEM analysis was conducted on Samples S5648 and S5696.

Run Nr.	***P*** **(GPa)**	***T*** **(°C)**	***t*** **(hrs)**	**Phase assemblage**
V791	5	1100	5	Fe_3O_4 + FeO
H3775	6	1000	3	Fe_3O_4 + FeO
S5827	6	1250	3	Melt + Fe_3O_4 + FeO
S5751	6	1100	5	Fe_3O_4 + FeO
S5727#	7	1000	5	Fe_3O_4 + FeO + Mo-oxide
S5982	7	1100		Fe_3O_4 + FeO
S5728#	8	1100	5	Fe_3O_4 + FeO + trace Fe_4O_5 + Mo-oxide
V733	8	1300	3	Melt + Fe_3O_4 + FeO
V734	8	1200	3	Fe_3O_4 + Fe_4O_5
V743	8	1000	5.5	Fe_3O_4 + Fe_4O_5
V736*	9	1200	7	Fe_4O_5
V744*	9	1000	5.5	Fe_3O_4 + Fe_4O_5
S5698*	9	1000	20	Fe_3O_4 + Fe_4O_5
H3551*	11	1000	7	Fe_4O_5
S5648*	12	1300	3	Fe_4O_5 + ReO_2
S5696*	12	1200	2	Fe_4O_5 + ReO_2
V739*	16	1100	3	Fe_4O_5
S5570*	16	1400	5	Fe_4O_5
S5640*	22	1000	5	Fe_3O_4 + Fe_4O_5
S5646*	22	1200	4	Fe_4O_5 + ReO_2

Table 2. Unit-cell lattice parameters determined for Fe_4O_5 synthesized at different pressures and temperatures. A small amount of Si was mixed with the sample and used as internal standard.

Run Nr.	Unit-cell lattice parameters Fe_4O_5			
	a (Å)	*b* (Å)	*c* (Å)	*V* (Å^3)
V734	2.8925 (2)	9.8067 (9)	12.5791 (12)	356.82 (5)
V744	2.9008 (3)	9.7994 (7)	12.5772 (7)	357.53 (4)
S5696	2.8932 (3)	9.8040 (14)	12.5785 (17)	356.79 (6)

Table 3. Thermodynamic data for FeO, Fe_4O_5 and Fe_5O_6-structured phases. Heat capacity parameters are in the form $(a+bT+cT^{-2}+dT^{-0.5})$. h-Fe_3O_4 from Lazor et al. (2004) is provided for completeness.

	Fe_4O_5	Fe_5O_6	$Mg_2Fe_2O_5$	FeO	$Fe_{2/3}\square_{1/3}O$	h-Fe_3O_4
H_0 [J/mol]	-1.342e6	-1.592e6	-1.987e6	-0.26545e6	-0.25517e6	-1.05746e6
S_0 [J/K/mol]	230	290	169.0	58	38.5	172.4
V_0 [m^3/mol]	5.376e-5	6.633e-5	5.305e-5	1.224e-5	1.107e-5	4.189e-5
K_0 [Pa]	1.857e11	1.730e11	1.700e11	1.52e11	1.52e11	2.02e11
K'_0 []	4	4	4	4.9	4.9	4
K''_0 [Pa^{-1}]	-2.154e-11	-2.312e-11	-2.353e-11	-3.2e-11	-3.2e-11	-
α_0 [K^{-1}]	2.36e-5	1.51e-5	2.36e-5	3.22e-5	2.79e-5	3.59e-5
C_p [J/K/mol]	306.9	351.3	284.9	42.64	54.63	262.5
	1.075e-3	9.355e-3	7.24e-4	8.971e-3	0.0	-7.205e-3
	3.1404e6	-4.3546e6	-3.3288e6	-0.2608e3	-0.7524e6	-1.9262e6
	-1.4705e3	-1.2853e3	-1.2560e3	-0.1966e3	-0.2192e3	-1.6557e3

Figure 1a

Click here to download Figure 01a.png

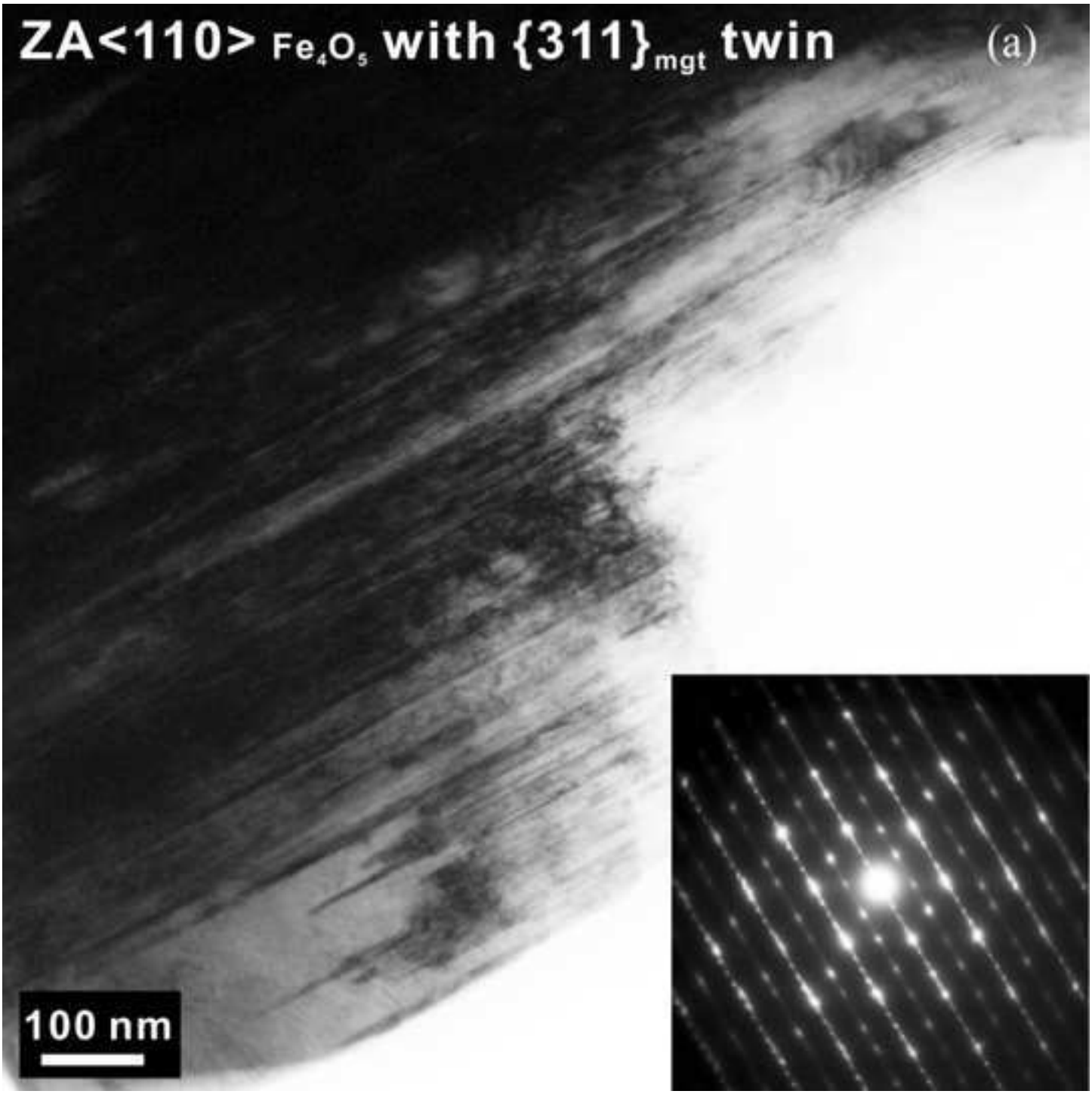

Figure 1b

Click here to download Figure 01b.png

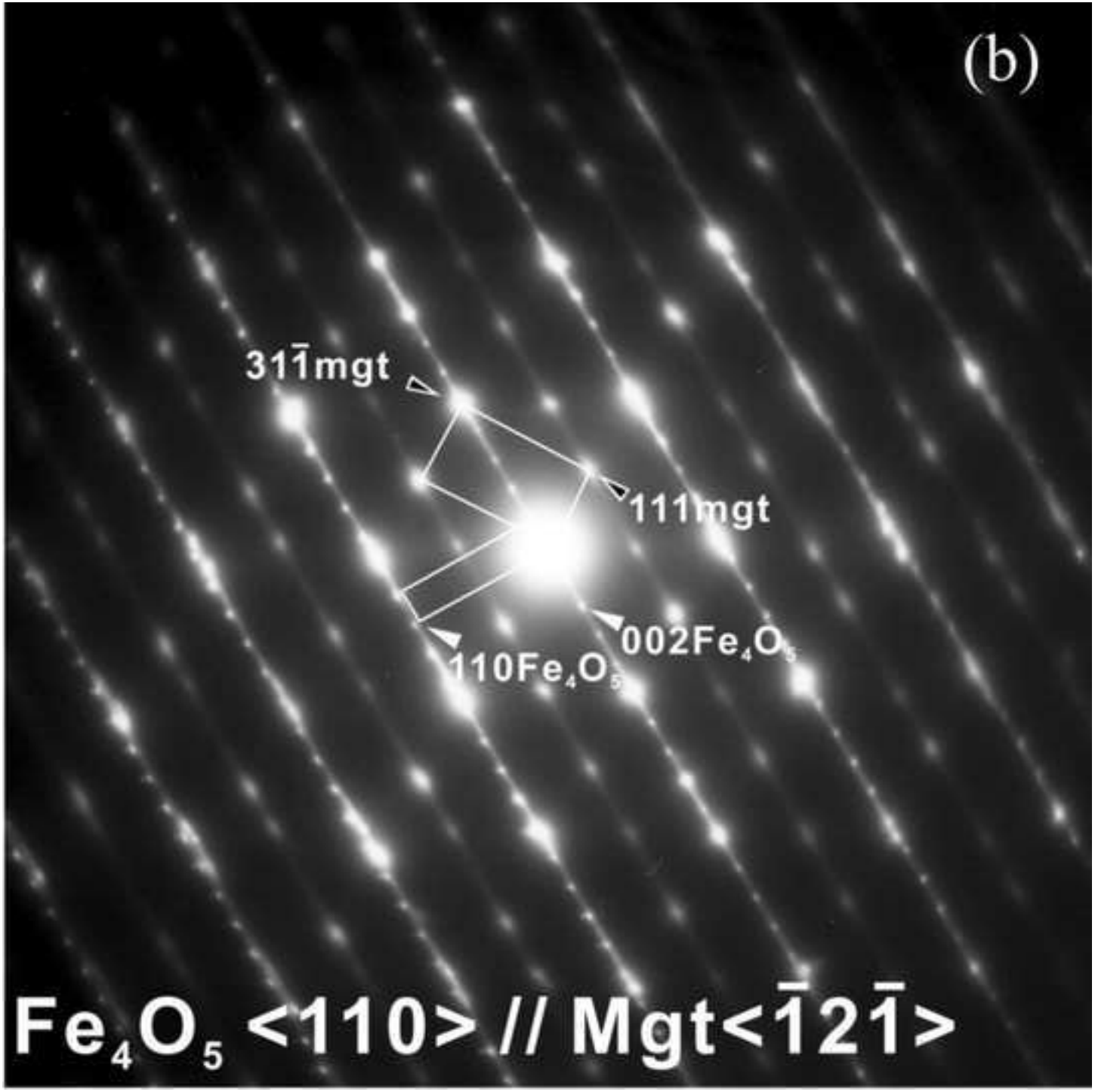

Figure 2

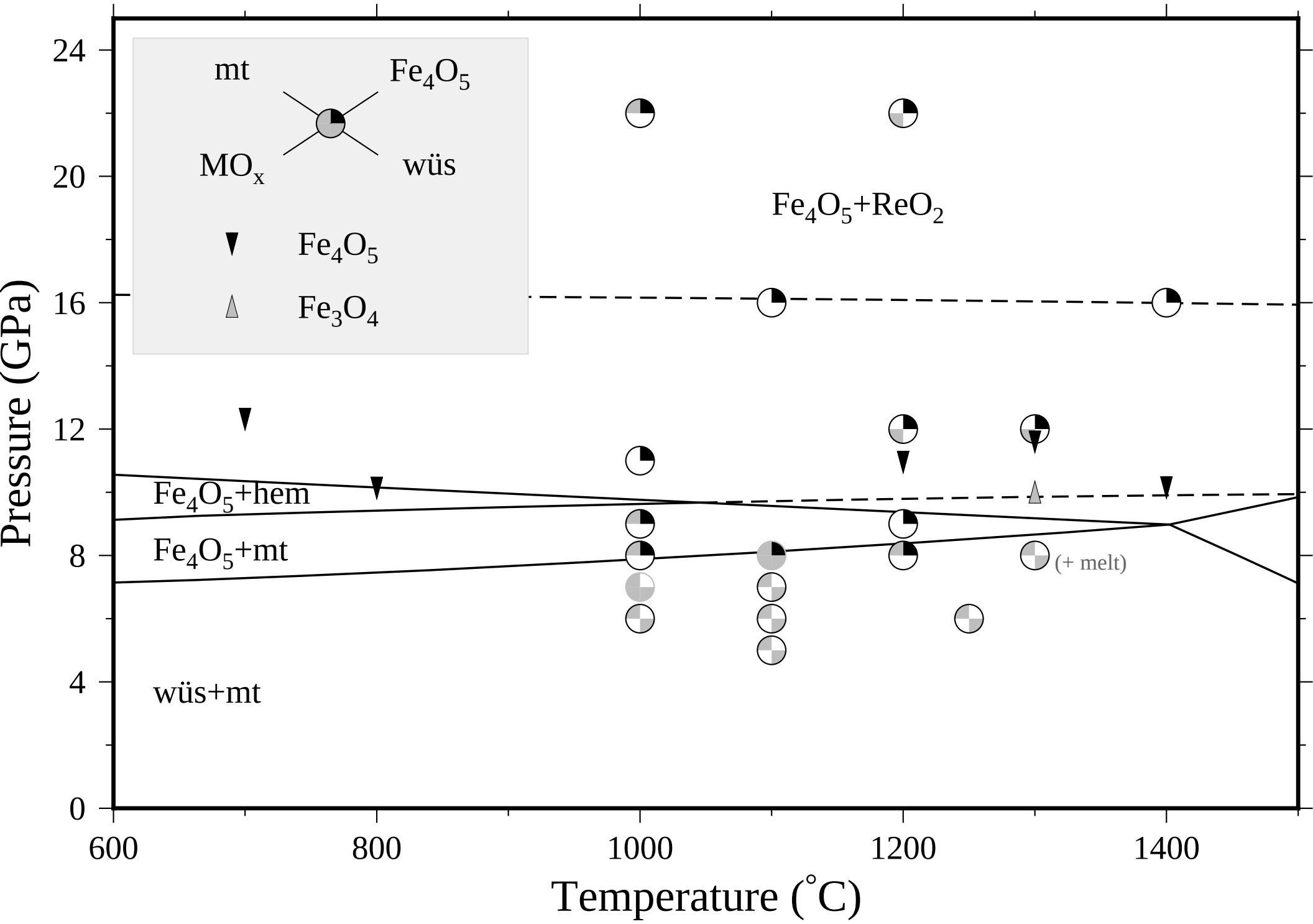

Figure 3

Click here to download Figure 03_P-fO2_simplified.eps

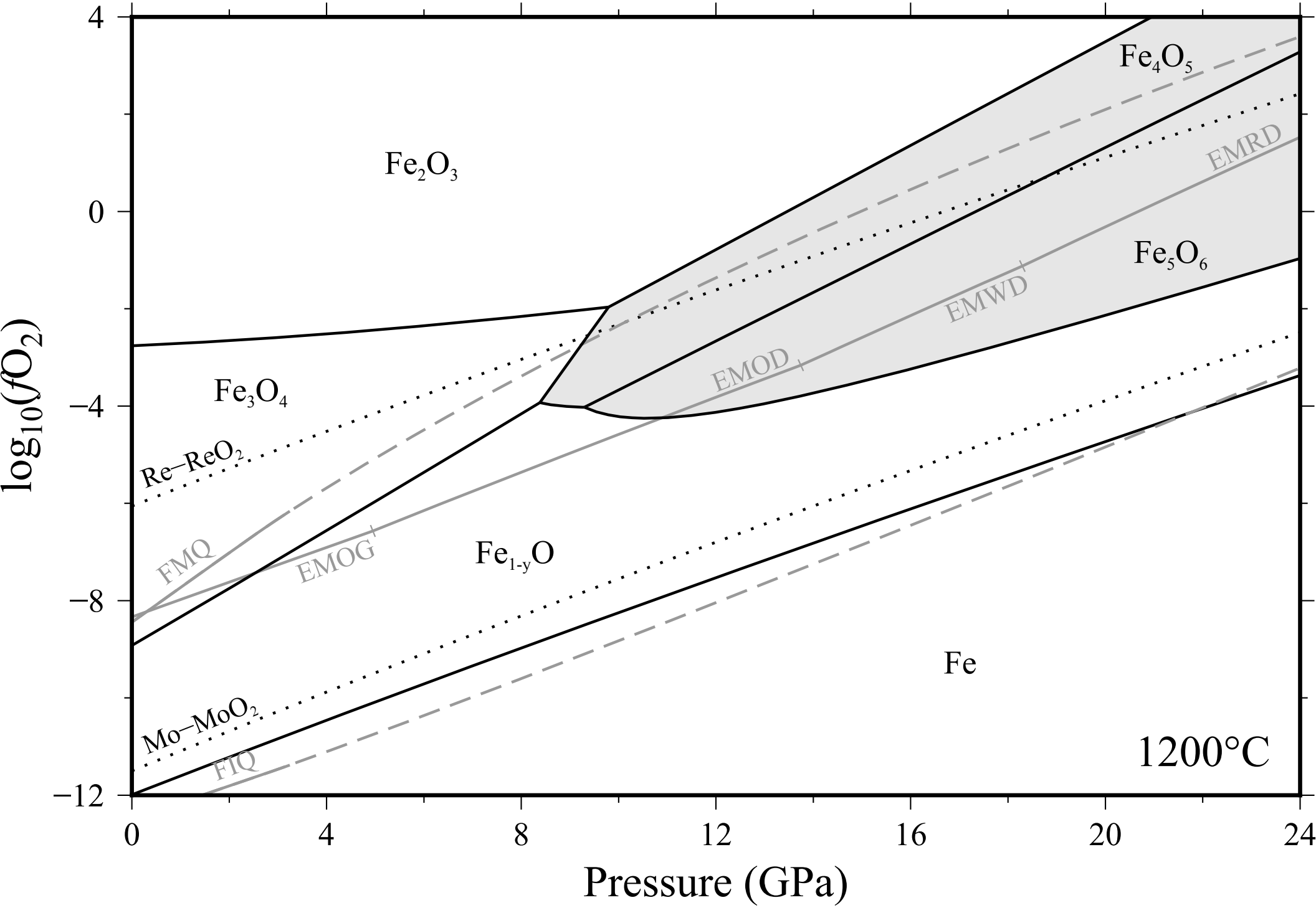

Figure 4

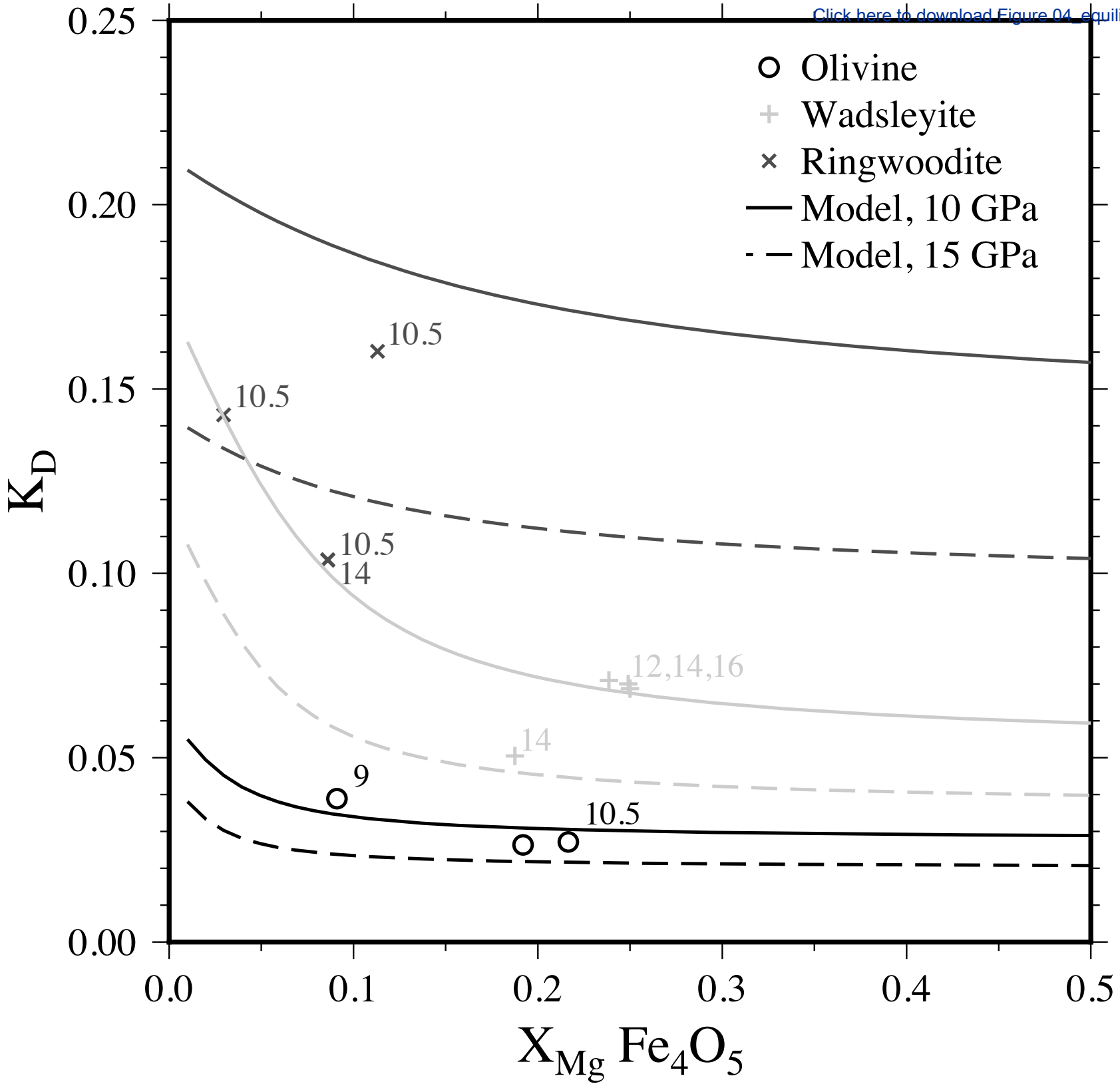

Figure 5

Click here to download Figure 05_ol_hpx_fe4o5.eps

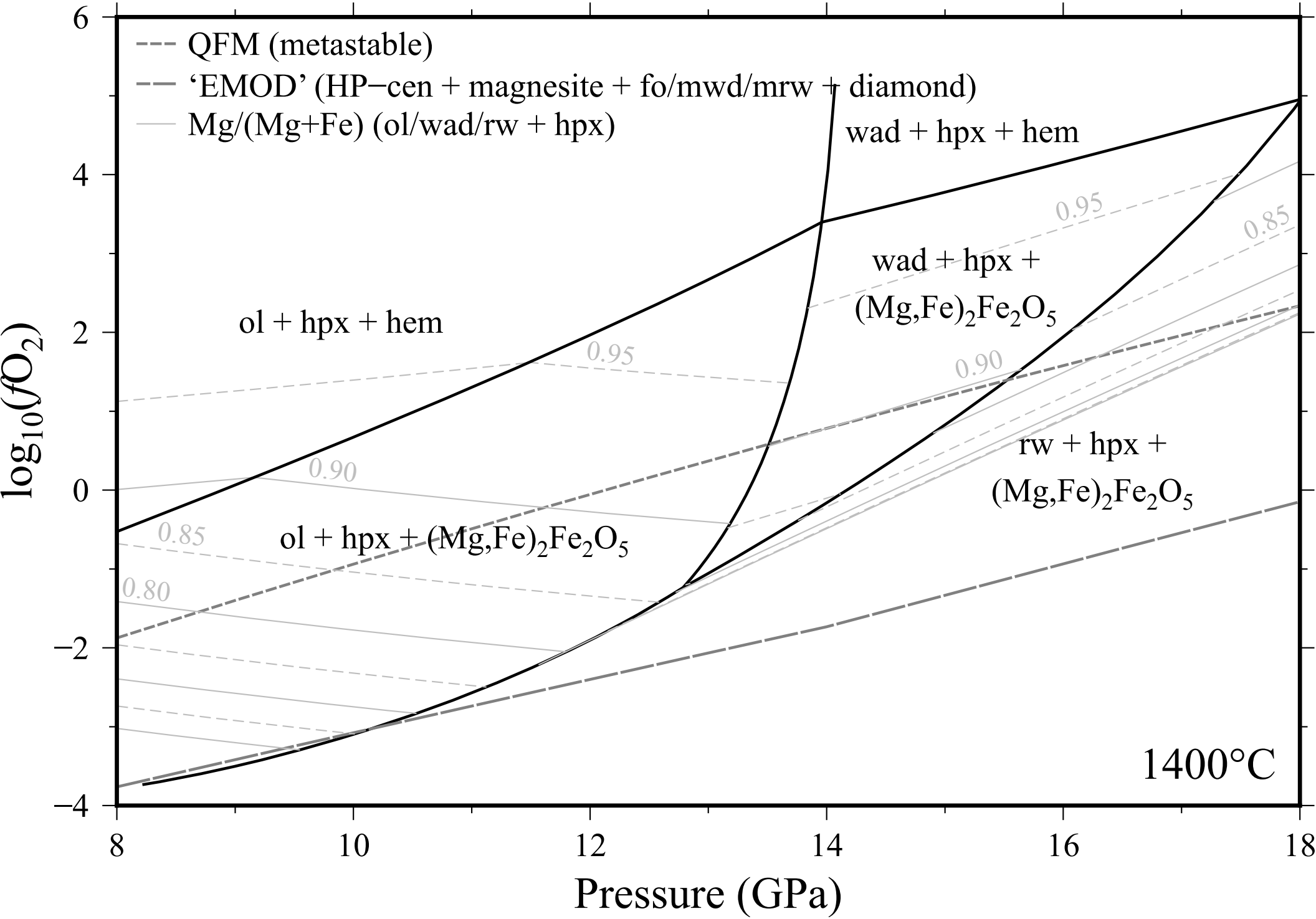

Figure 6

Click here to download Figure 06_gt_compositions.eps